

Magnetic Skyrmionic Polarons

Luis Brey*

Instituto de Ciencia de Materiales de Madrid, CSIC, 28049 Cantoblanco, Spain

E-mail: brey@icmm.csic.es

Abstract

We study a two-dimensional electron gas exchanged-coupled to a system of classical magnetic ions. For large Rashba spin-orbit coupling a single electron can become self-trapped in a skyrmion spin texture self-induced in the magnetic ions system. This new quasiparticle carries electrical and topological charge as well as a large spin, and we named it as magnetic skyrmionic polaron. We study the range of parameters; temperature, exchange coupling, Rashba coupling and magnetic field, for which the magnetic skyrmionic polaron is the fundamental state in the system. The dynamics of this quasiparticle is studied using the collective coordinate approximation, and we obtain that in presence of an electric field the new quasiparticle shows, because the chirality of the skyrmion, a Hall effect. Finally we argue that the magnetic skyrmionic polarons can be found in large Rashba spin-orbit coupling semiconductors as GeMnTe.

Keywords: Magnetic Skyrmions, Polarons, Magnetic Semiconductors

In 1962 Skyrme introduced a model where particles as photons and neutrons show up as topological defects of fields of mesons.¹ These particles were named skyrmions and also appear as topological excitations in the continuum limit of the two-dimensional (2D) ferromagnetic Heisenberg model; the celebrated non-linear sigma model (NLSM),² $H_{NLSM} = \frac{\rho_s}{2} \int \partial_\alpha \mathbf{n} \cdot \partial_\alpha \mathbf{n} d^2\mathbf{r}$. Here \mathbf{n} is the magnetization unit vector and ρ_s is the spin stiffness. The NLSM is scale invariant and the energy of the skyrmion, $4\pi\rho_s$, does not depend on its size or on a global spin rotation.³ By extension, the term skyrmion is also used to name topological excitations of two component scalar field in 2D systems. In these cases extra terms added to the NLSM make the energy, shape and size of the skyrmions depend on the details of the Hamiltonian. Apart from nuclear physics⁴ skyrmions appear in many brands of modern physics⁴ as two-dimensional electron gas in the quantum Hall regime,^{5,6} liquid crystals,⁷ Bose-Einstein condensates⁸ and in the last years the study of skyrmions has convulsed the research of magnetic materials.⁹⁻¹⁶

In 2D ferromagnetic systems, a magnetic skyrmion describes a localized spin texture, where in going from the core to the perimeter of the particle, the orientation of the spin full wraps the unit sphere. The topology of the skyrmion is characterized by a nonzero topological charge,

$$Q = \frac{1}{4\pi} \int \mathbf{n}(\mathbf{r}) \cdot [\partial_x \mathbf{n}(\mathbf{r}) \times \partial_y \mathbf{n}(\mathbf{r})] d\mathbf{r} \quad (1)$$

that indicates the number of times the unit sphere is wrapped by the magnetization $\mathbf{n}(\mathbf{r})$, when this covers the full real space. The topological character of the skyrmions protects them from continuous deformation into the uniform and conventional ferromagnetic state, conferring them a long lifetime. This protection, in addition with the experimental fact that skyrmions can be driven by low electrical current densities,¹⁷ makes them very promising particles for spintronic devices.^{18,19} Different mechanisms¹⁵ as long-ranged magnetic dipolar interactions,²⁰ frustrated exchange interactions²¹ or four-spin exchange mechanism,²² can produce stable skyrmions in magnetic systems. Very interesting are the skyrmions that appear in non-centrosymmetric magnets, where the competition between

an antisymmetric Dzyaloshinskii-Moriya (DM) interaction^{23,24} and a symmetric exchange coupling can generate, in presence of an external magnetic field, skyrmions with size ranging from 5 to 100nm. The origin of the DMI is the lack of inversion symmetry in lattices or at the interface of magnetic films. In ultrathin magnetic films the DMI appear as the exchange coupling between two atomic spins mediated by a heavy atom with a large spin-orbit coupling (SOC).^{25,26} The DMI between classical spins can also occurs as a modified Ruderman-Kittel-Kasuya-Yosida²⁷⁻²⁹ interaction, where the intermediary 2D electron gas has a Rashba SOC.³⁰⁻³² Double exchange magnetic metals³³ with strong SOC may also generate DM interaction between the magnetic ions.^{32,34}

In diluted magnetic semiconductors a single electron is able to create a ferromagnetic collective ground state of a large number of magnetic impurities.^{35,36} Also there is evidence³⁷⁻³⁹ that a single electron can be self-trapped in a magnetic polaron. The question then arises is if a single electron with Rashba spin-orbit coupling can be self-trapped in a spin texture induced in a coupled system of magnetic ions. By combining analytical calculations and numerical computation, we find compelling evidence that the Rashba spin orbit coupling makes that a single electron creates and becomes self trapped in a skyrmion spin texture. We name this quasiparticle as *magnetic skyrmionic polaron*.

The Hamiltonian for electrons moving in the conduction band of a 2D semiconductor in the presence of a unit vector magnetization is

$$H = \frac{\hbar^2 \mathbf{k}^2}{2m^*} + \alpha (\sigma_x k_y - \sigma_y k_x) - J \mathbf{n}(\mathbf{r}) \cdot \boldsymbol{\sigma} - \bar{b}_z \int n_z(\mathbf{r}) d\mathbf{r} \quad (2)$$

where σ_x , σ_y and σ_z are the Pauli matrices and J is the exchange coupling constant that we consider positive. In the Hamiltonian we also have included a Zeeman field, \bar{b}_z , acting on the magnetic impurities. In Eq.2 m^* is the effective mass and α the Rashba SOC.

Different trivial uniform states can surge from the coupling between the electron spin and the magnetic impurities. For $J=\bar{b}_z=0$, the energy of the electron is $\epsilon = \frac{\hbar^2}{2m^*} (k - k_R)^2 - \frac{\hbar^2 k_R^2}{2m^*}$ with $k_R = \frac{m^*}{\hbar^2} \alpha$ and the minimum occurs at the ring defined by $k=k_R$. Because of

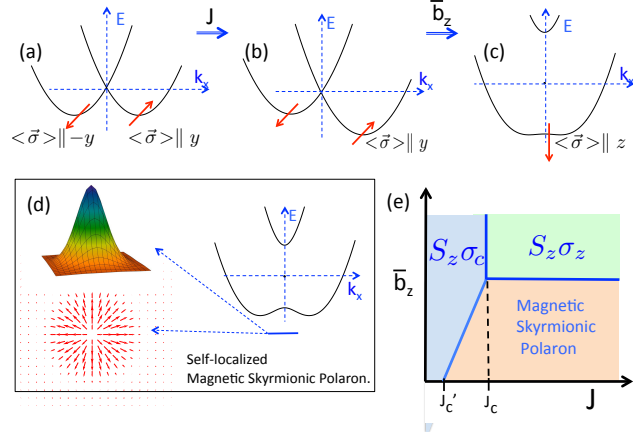


Figure 1: Schematic picture of the band structure corresponding to the phases (a) $S_z \sigma_c$, (b) $S_\perp \sigma_\perp$ and (c) $S_z \sigma_z$, see text. In (d) we indicate how an electron can be self-trapped in a magnetic skyrmionic polaron, with energy below the bottom of the band, and with the wave function located on the spin texture. In (e) we show a typical phase diagram obtained by minimizing Eq.5.

the SOC, the spin of a state with momentum $k_R(\cos \beta, \sin \beta)$, points in the direction $\langle \vec{\sigma} \rangle = (-\sin \beta, \cos \beta, 0)$. For $\bar{b}_z = 0$ and finite coupling between the electron spin and the magnetic ions, $J \neq 0$, a single electron selects an in-plane magnetic orientation for the system of magnetic ions. We call this phase $S_\perp \sigma_\perp$, Figure 1(b). For $J \neq 0$ and $\bar{b}_z \neq 0$, $\mathbf{n}(\mathbf{r})$ polarizes along the z -direction and the electron spin orientation gets a component along the z -direction, canted phase $S_z \sigma_c$, until that for $J > J_c = \frac{\hbar^2 k_R^2}{2m^*}$, both the electron spin and $\mathbf{n}(\mathbf{r})$ become polarized in the z -direction in a phase we call $S_z \sigma_z$, Figure 1(c). In this work we study the transition, as function of \bar{b}_z , between the $S_\perp \sigma_\perp$ and the $S_z \sigma_z$ phases and show that the electron can be self-trapped by a skyrmion induced in the coupled magnetic ion system, forming a magnetic skyrmionic polaron, Figure 1(d).

Effective spinless Hamiltonian. Here we consider a single electron in presence of a $Q=1$ skyrmion of the form,

$$\mathbf{n}(\mathbf{r}) = (\cos \theta \sin \xi(r), \sin \theta \sin \xi(r), \cos \xi(r)) \quad (3)$$

where θ is the polar angle and $\xi(r)$ is a continuous function satisfying $\xi(r = 0) = \pi$

and $\xi(r \rightarrow \infty)=0$, and we minimize the energy of the system with respect to the size of the skyrmion. We use an unitary transformation of the Hamiltonian which makes the spin quantization direction parallel to the direction of the magnetization $\mathbf{n}(\mathbf{r})$,⁴⁰⁻⁴² i.e. $U^\dagger \mathbf{n}(\mathbf{r}) \boldsymbol{\sigma} U = \sigma_z$ with $U = \begin{pmatrix} u_1^* & -u_2^* \\ u_2 & u_1 \end{pmatrix}$, being $u_1 = \cos \frac{\xi(r)}{2} e^{i\theta/2}$ and $u_2 = \sin \frac{\xi(r)}{2} e^{i\theta/2}$. We are interested in the zero density limit in which J is the largest energy in the system and we neglect electrons with spin locally antiparallel to the magnetization $\mathbf{n}(\mathbf{r})$. In this approximation we obtain the following Hamiltonian for spinless electrons,

$$H' = \frac{\hbar^2}{2m^*} \left(\mathbf{k} - \frac{e}{\hbar c} \mathbf{a} \right)^2 + \frac{\hbar^2}{8m^*} \left(\frac{\partial \xi(r)}{\partial r} \right)^2 + \alpha \left(\frac{1}{2} \frac{\partial \xi(r)}{\partial r} + i \frac{\sin \xi(r)}{r} \frac{\partial}{\partial \theta} \right) - J - \bar{b}_z \int n_z(\mathbf{r}) d\mathbf{r}, \quad (4)$$

$$\text{with } \phi_0 = \frac{\hbar c}{e} \text{ and } \mathbf{a}(\mathbf{r}) = \frac{\phi_0 \cos \xi(r)}{4\pi r^2} (y, -x).$$

The first two terms in H' contain the coupling between the electron and the gauge vector potential and electrostatic potential generated by the spatial variation of the order parameter $\mathbf{n}(\mathbf{r})$, respectively. The third has its origin in the rotation of the Rashba term. The vector potential $\mathbf{a}(\mathbf{r})$ describes a topological magnetic field $B_t = \partial_x a_y - \partial_y a_x = \frac{\phi_0 \sin \xi(r)}{4\pi r} \frac{\partial \xi(r)}{\partial r}$, that is proportional to the density of topological charge in the spin texture. The skyrmion profile is well modeled⁴³ as $\xi(r) = \pi(1 - r/\lambda)$ for $r < \lambda$ and $\xi(r) = 0$ for $r > \lambda$, that describes a smooth radial spin texture inside the skyrmion radius λ . For this profile, $\frac{\partial \xi(r)}{\partial r} = -\pi/\lambda$, for $r < \lambda$ and zero elsewhere, then the second and third term of H' describe a quantum dot of radius λ and potential $\frac{\hbar^2}{8m^*} \frac{\pi^2}{\lambda^2} - \alpha \frac{\pi}{2\lambda}$. The average topological magnetic field takes a value $\bar{B}_t = \frac{1}{\pi} \frac{\phi_0}{\lambda^2}$ that implies a magnetic length $\ell = \lambda/\sqrt{2}$ smaller than the dot radius and therefore an electron located on the skyrmion should have a zero point motion energy $\frac{\hbar \omega_c}{2} \sim \frac{\hbar^2}{2m^*} \frac{2}{\lambda^2}$. Adding all contributions the energy of the system is,

$$E \simeq \frac{\hbar^2}{2m^*} \left(\frac{\pi^2}{4} + 2 \right) \frac{1}{\lambda^2} - \alpha \frac{\pi}{2\lambda} - J + 2\pi \bar{b}_z \lambda^2 \left(\frac{1}{2} - \frac{2}{\pi^2} \right). \quad (5)$$

Minimizing this equation with respect the radius of the skyrmion, we obtain that for small values of the Zeeman field, there is always a negative energy solution that corresponds to the self trapping of the electron in a self-induced skyrmion spin texture. At $\bar{b}_z=0$ the radius of the skyrmion is $\lambda \approx \frac{3\hbar^2}{m^*\alpha}$, and decreases as \bar{b}_z increases.

We call this quasiparticle a *magnetic skyrmionic polaron*. This particle competes in energy with the non-topological states $S_\perp\sigma_\perp$, $S_z\sigma_c$ and $S_z\sigma_z$. A typical phase diagram is shown in in Figure 1(e). At large values of \bar{b}_z and J all spins polarize in z -direction and the ground state is $S_z\sigma_z$, for large values of \bar{b}_z but moderate values of J , the magnetic ions polarize in the z -direction, but the electron spin is canted, phase $S_z\sigma_c$. For large values of J and moderate values of \bar{b}_z the electron self-traps in a magnetic skyrmionic polaron. At $\bar{b}_z=0$, the transition between the $S_z\sigma_c$ and the magnetic polaronic phase occurs at J'_c . The difference between J'_c-J_c is the binding energy of the magnetic skyrmionic polaron at $\bar{b}_z=0$.

The results obtained from the effective spinless Hamiltonian Eq.4, provide a physical insight of how an electron can be self-trapped in a skyrmion. In the following we perform tight-binding calculations in order to check the validity of the previous conclusions and also for studying a wider range of values of the exchange coupling J and obtain a more accurate description of the magnetic skyrmionic polarons. We consider a square lattice, first-neighbors hopping tight-binding Hamiltonian,⁴⁴

$$\begin{aligned}
H &= -t \sum_{i,j,\sigma} c_{i,\sigma}^+ c_{j,\sigma} + t_R \left(\sum_j -i (c_{j,\uparrow}^+ c_{j+a_y,\downarrow} + c_{j,\downarrow}^+ c_{j+a_y,\uparrow}) + \right. \\
&\quad \left. (c_{j,\uparrow}^+ c_{j+a_x,\downarrow} - c_{j,\downarrow}^+ c_{j+a_x,\uparrow}) + h.c. \right) - J \sum_i \mathbf{S}_i \boldsymbol{\sigma}_i - b_z \sum_i S_{i,z}
\end{aligned} \tag{6}$$

where $c_{i,\sigma}^+$ creates an electron at site i with spin σ , $t=\hbar^2/2m^*a^2$, $t_R=\alpha/2a$, $\boldsymbol{\sigma}_i=c_{i,\alpha}^+ \boldsymbol{\sigma}_{\alpha,\beta} c_{i,\beta}$ is the electron spin operator, \mathbf{S}_i is the impurity spin normalized to unity and $\vec{\delta}=(\pm a\hat{x}, \pm a\hat{y})$, being a the lattice spacing. We consider a single electron in a supercell containing $N \times N$ sites and use periodic boundary conditions, so that the density of charge in the system

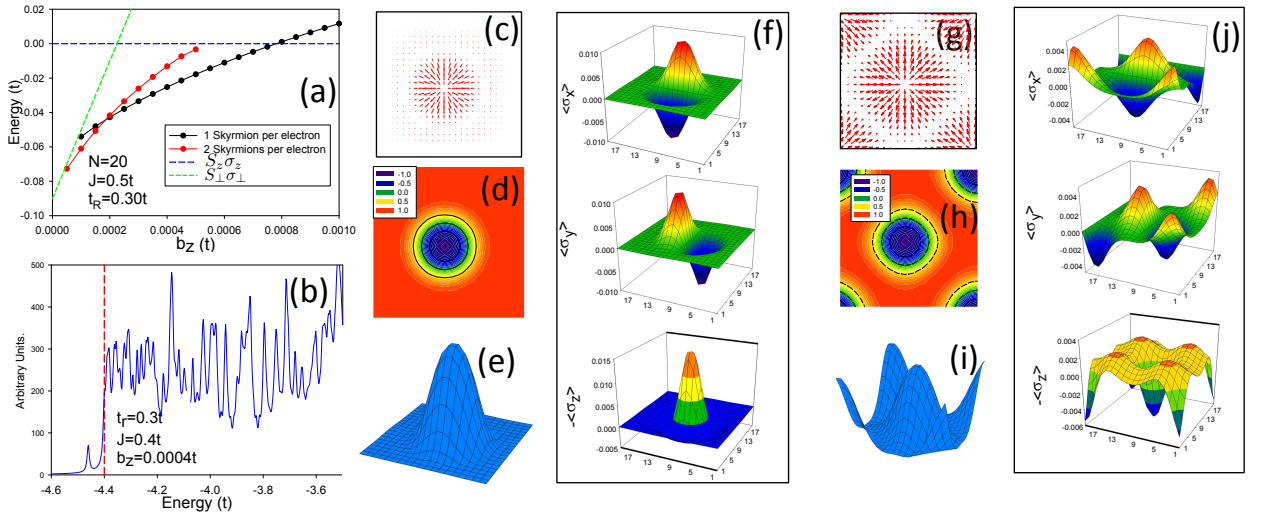


Figure 2: (a) Energy of different states, as function of b_z , for $J=0.5t$, $t_R=0.3t$, and $N = 20$, as obtained from tight-binding calculations.. The energies are plotted with respect the energy of the $S_z\sigma_z$ state. (b) Electron density of states for the case $b_z=0.0005t$, $J=0.4t$, $t_R=0.3t$, and $N = 50$. The vertical red line indicated the position of the bottom of the electronic band. The sharp peak below the band correspond to the magnetic skyrmionic polaron. (c) and (d) show the spin texture corresponding to a $Q=1$ skyrmion at $b_z=0.0005t$, the other parameters the same than in (a). In (e) we plot the topological charge density for the same parameters than in (c). In (g)-(j) we plot the same magnitudes than in (c)-(f) for the case $Q=2$ and $b_z=0.0002t$.

is $\frac{1}{N^2 a^2}$. The Hamiltonian Eq.6 is solved self consistently in a process where after diagonalizing and obtaining the wave-function of the lowest energy state in presence of a spin texture, we recalculated the spin texture created by the expectation value of the electron spin operator and b_z and then repeat the process until input and output coincide. Solving Eq.6, we obtain the electron energy and wave-function, as well that the orientation of the magnetic ions $\{\mathbf{S}_i\}$. For a given spin configuration the topological charge is obtained by following the prescription of Berg and Lusher.⁴⁵ We divide each basic unit square of the lattice into two triangles. The three spins at the corners of each triangle l define a signed area on the unit sphere A_l , and the topological charge in the supercell is given by $Q=1/4\pi \sum_l A_l$, where the sum runs over all triangles in the system.

By starting the self-consistent procedure with seeds corresponding to different spin textures, we obtain solutions with different topological charge in the unit cell. In the tight-binding calculation we do not impose any constrain to the size and shape of the skyrmions. In Figure 2(a) we plot the energy per unit cell of different states for the case $t_R=0.3t$, $J=0.5t$ and $N=20$, as function of the Zeeman field b_z . For these large values of J , the relevant uniform non-topological phases are $S_z\sigma_z$, with energy $-4t-J-N^2b_z$ that is the ground state for large values of b_z and $S_\perp\sigma_\perp$ with energy $-4t-t_R^2/t-J$ that is the relevant phase for $N^2b_z < t_R^2/t$. We see in Figure 2(a) that there is a range of Zeeman fields for which the low energy state corresponds to a $Q=1$ magnetic skyrmionic polaron. This is evident in Figure 2(c)-(d) where we plot the $x-y$ and the z -component of the ion spins for $J=0.5t$, $t_R=0.3t$ and $b_z=0.0005t$. Clearly, there is an isolated skyrmion located at the center of the unit cell. The coupling between the electron and the magnetic ions is also reflected in the electron spin density shown in Figure 2(f), that shows the same symmetry and shape than the ions spin texture. The self-trapping of the electron by the skyrmion and the binding energy is also reflected in the electron density of states, Figure 2(b); below the bottom of the electron band, $-4t-J$, there appears a sharp peak containing exactly one electron and that corresponds to the magnetic skyrmionic polaron. In Figure 2(a) we notice that at very low Zeeman fields, the low energy phase corresponds to a

topological charge $Q=2$ in the unit cell. This phase occurs because for small values of b_z , the size of the skyrmion increases and skyrmions centered in neighbor unit cells overlap and interact, being energetically favorable for the system to create a skyrmion crystal with two $Q=1$ skyrmions per unit cell, Figure 2(g)-(i), and a single electron per unit cell Figure 2(j).

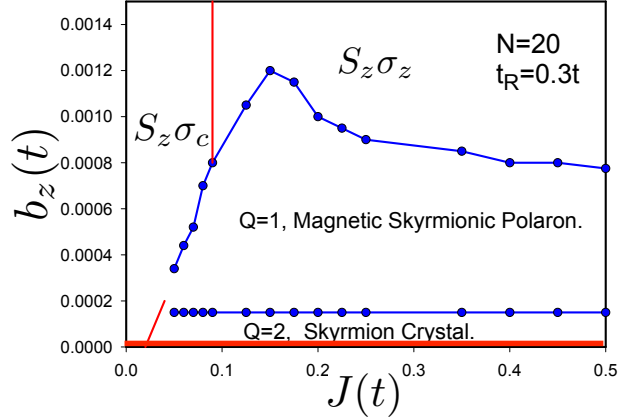


Figure 3: Phase diagram, b_z versus J , for $t_R=0.3t$ and calculated in a supercell with $N=20$. The phase $S_{\perp}\sigma_{\perp}$ phase corresponds to the thick red line, and it is the ground state at very small values of N^2b_z .

In Figure 3 we show a phase diagram b_z versus J , for $t_R=0.3t$ obtained in a supercell with $N=20$. The main differences when comparing with the obtained in the effective spinless Hamiltonian, Figure 1(e) are, first there is a small but finite region of values of b_z where the ground state is $S_{\perp}\sigma_{\perp}$ and second, by increasing b_z in the transition from the $S_{\perp}\sigma_{\perp}$ state to the magnetic skyrmionic polaron phase, there appears a region where there are two skyrmions per electron, crystallizing in a square lattice. Both effects occur because of the small size of the unit cell, the energy associated with the polarization of the magnetic ions in the z -direction is $b_z N^2$, and therefore as larger is N , smaller is the region in the J - b_z parameter space where $S_{\perp}\sigma_{\perp}$ is the ground state. In the same way, as N increases the overlap between magnetic skyrmionic polaron decreases and the $Q=2$ region disappears in the phase diagram.

Dynamics of magnetic skyrmionic polarons. The dynamics of the impurity spins, treated

as classical, is dictated by the Landau-Lifshitz equation,⁴⁶

$$\partial_t \mathbf{S}_i = \frac{1}{\hbar} \mathbf{H}_i \times \mathbf{S}_i + \alpha_G \mathbf{S}_i \times \partial_t \mathbf{S}_i \quad (7)$$

where $\alpha_G \ll 1$ is the phenomenological Gilbert damping constant and \mathbf{H}_i is the local effective field, written in energy units, that is derived from the Hamiltonian, $\mathbf{H}_i = -\frac{\partial H}{\partial \mathbf{S}_i}$. In the previous equation we have not included a current-induced torque because although the spin texture is charged it is placed in an insulator materials.^{47,48} Equation 7 describes both the deformation and the dynamics of the skyrmions. The excitation of the internal modes of the skyrmions have a finite frequency, that increases with the presence of an external magnetic field and this justifies the treatment of skyrmions as rigid particles,⁴⁹ that move across the sample without distortion. Therefore, the dynamics of skyrmions is defined by the position (X, Y) and velocity (V_x, V_y) of its center of mass. The motion of the center of mass is obtained by integrating the Landau-Lifshitz equations following the method developed by Thiele,⁵⁰⁻⁵² and for a magnetic texture as that described in Eq.3 we obtain,

$$\begin{aligned} F_x &= -GMV_y + \alpha_G MDV_x \\ F_y &= GMV_x + \alpha_G MDV_y, \end{aligned} \quad (8)$$

here M is the magnetic moment per unit area in the magnetic system, $G=4\pi Q$, $D=\pi \int_0^\infty dr \left(\frac{\sin^2 \xi(r)}{r} + \dots \right)$ and \mathbf{F} is the so called generalized force acting on the skyrmion due to impurities, magnetic fields or boundary conditions.¹⁵ Magnetic skyrmionic polarons are charged particles and therefore they also respond to electromagnetic fields. In the case of an electric field $E=(E_x, 0)$, the skyrmion acquires a velocity,

$$V_x = \frac{\alpha MD}{(\alpha_G MD)^2 + M^2 G^2} e E_x \quad (9)$$

$$V_y = -\frac{MG}{(\alpha_G MD)^2 + M^2 G^2} e E_x. \quad (10)$$

The magnetic skyrmionic polaron steady velocity in the direction of the electric field is determined by the balance between electric field and damping. In the limit of vanishing damping the particle shows a Hall effect with $V_x=0$ and $V_y=\mu E_x$, that defines a mobility $\mu=-e/MG$, that for a density of magnetic moments of the order of \hbar/nm^{-1} takes values $\mu \sim 1 \times 10^{-4} \text{m}^2/\text{Vs}$ that implies drift velocities $v_H \sim 0.01 \text{m/s}$ for applied electric fields $E_x=10^2 \text{eV/m}$, comparable or larger to that of magnetic skyrmions driven by electric current.^{53,54} Large drift velocities have been also predict for skyrmions placed on top of topological insulators.⁵⁵

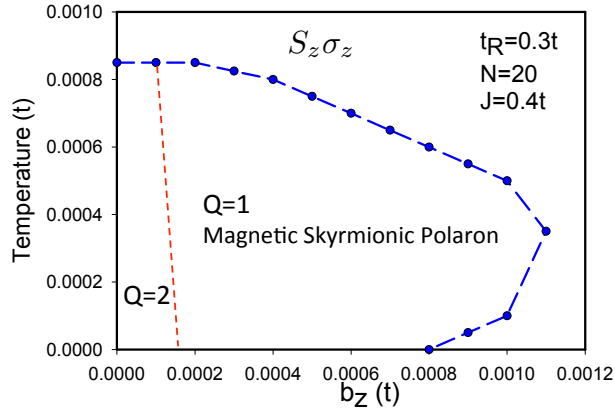


Figure 4: Temperature- b_z , phase diagram, for $t_R=0.3t$, $J=0.4t$ and calculated in a super-cell with $N=20$.

We estimate the effect of the temperature on the existence of magnetic skyrmionic polarons in the mean field approximation. The effective magnetic field acting on the normalized spin impurity \mathbf{S}_i is,

$$\mathbf{B}_i = (-J \langle \sigma_{x,i} \rangle, -J \langle \sigma_{y,i} \rangle, -J \langle \sigma_{z,i} \rangle - b_z), \quad (11)$$

where $\langle \sigma_i \rangle$ us the expectation value of the electron spin operator at site i . In the mean field approximation the free energy of classical spin S_i is,

$$\mathcal{F}_i = -k_B T \ln \left[2 \frac{\sinh(B_i/k_B T)}{B_i/k_B T} \right] \quad (12)$$

from which the expectation value of the spin impurity is⁵⁶

$$\langle \mathbf{S}_i \rangle = \langle S_i \rangle \frac{\mathbf{B}_i}{B_i} \text{ with } \langle S_i \rangle = \frac{1}{\tanh(B_i/k_B T)} - \frac{k_B T}{B_i}. \quad (13)$$

By solving self-consistent Eq.6, with the values of the ion spin \mathbf{S}_i replaced by $\langle \mathbf{S}_i \rangle$, Eq.13, we obtain the temperature phase diagram for the occurrence of magnetic skyrmionic polarons. In this approximation we assume that the magnetic skyrmionic polaron binding energy is larger than the temperature and the only participating electron state is that with lowest energy. The main effect of temperature is the reduction of the expectation value of the classical spins, that results in an effective reduction of the Rashba spin orbit coupling in Eq.6. In Figure 4 we plot the phase diagram temperature- b_z for the parameters $t_R=0.3t$, $J=0.4t$ and a unit cell $N = 20$. When increasing temperature the reduction of the effective Rashba coupling induces a transition from the skyrmionic phase to the $S_z\sigma_z$ phase. The reentrance of the $S_z\sigma_z$ phase at large values of b_z reflects the maxima occurring in the b_z - J phase diagram, Eq.3.

In closing, in this paper we have shown, using analytical estimations and numerical calculations, that a single electron moving in a band with a strong Rashba spin-orbit coupling and coupled to magnetic ions can be self-trapped by forming a skyrmion spin texture. We have calculated the phase diagram for the existence of this magnetic skyrmionic polaron, as function of the exchange coupling, Rashba SOC, temperature and external magnetic field. Also, we have analyzed the dynamics of the skyrmionic polaron and found that in presence of an electric field, the skyrmion will show a Hall effect with a rather large mobility and drift velocity.

In this work we have studied a 2D semiconductor in the limit of very low electron density. For higher electron densities, a well-defined RKKY interaction between magnetic impurities should develop. In the presence of Rashba spin-orbit coupling, this interaction should induce effective exchange and DM interactions between the ion spins. In this high-density regime, a phase diagram with a helical, ferromagnetic and skyrmion crystal

phases, as that presented in ref.,³² is expected. In this high density regime, the skyrmions in the crystal phase should overlap strongly and the resulting electronic density should be slightly modulated with a small charge accumulation near the skyrmion core.⁵⁷

The existence of magnetic skyrmionic polaron requires a semiconductor with a large Rashba SOC and a large exchange coupling between the electron spin and the magnetic ions. Recently it has been reported soft X-ray ARPES on epitaxially grown thin films of $\text{Ge}_{1-x}\text{Mn}_x\text{Te}$.⁵⁸ For a concentration $x=5.4\%$ of Mn, the measured band structure parameters are, $m^*=0.2$, $\lambda=3\text{eV}\text{\AA}$, and $J=0.11\text{eV}$, that correspond to the following tight-binding parameters, $t=0.53\text{eV}$, $t_R=0.25\text{eV}$ and $J=0.06\text{eV}$ obtained using a lattice constant $a \sim 6\text{\AA}$.⁵⁹ From these numbers, and comparing with the results presented in Figure 2 and Figure 3 we conclude that it is possible that magnetic skyrmionic polarons appear in $\text{Ge}_{1-x}\text{Mn}_x\text{Te}$ at very low densities and temperatures lower than 10K. For a concentration of Mn ions of 5% the magnetic skyrmionic polarons will be present up to rather large magnetic fields, $>20\text{T}$. Recently obtained quasi two-dimensional ferromagnetic materials,⁶⁰⁻⁶² are expected to have a strong Rashba spin orbit coupling and therefore are also good candidates to host magnetic skyrmionic polarons.

Acknowledgement

Author acknowledges H.A.Fertig for helpful discussions. This work has been partially supported by the Spanish MINECO Grant No. FIS2015-64654-P.

References

- (1) Skyrme, T. H. R. *Nuclear Physics* **1962**, *31*, 556-569.
- (2) Belavin, A. A.; Polyakov, A. M.; Zamolodchikov, A. B. *Nucl. Phys.* **1984**, *B241*, 333-380.

- (3) A.Rajaraman, *An Introduction to Solitons and Instantons in Quantum Field Theory*; Elsevier, 1987.
- (4) G.E.Brown,, Rho, M., Eds. *The Multifaceted Skyrmion*; World Scientific, 2010.
- (5) Fertig, H. A.; Brey, L.; Côté, R.; MacDonald, A. H. *Physical Review B* **1994**, *50*, 11018–11021.
- (6) Brey, L.; Fertig, H. A.; Côté, R.; MacDonald, A. H. *Physical Review Letters* **1995**, *75*, 2562–2565.
- (7) Fukuda, J.-i.; Žumer, S. *Nature Communications* **2011**, *2*, 246 EP –.
- (8) Al Khawaja, U.; Stoof, H. *Nature* **2001**, *411*, 918–920.
- (9) Roszler, U. K.; Bogdanov, A. N.; Pfeleiderer, C. *Nature* **2006**, *442*, 797–801.
- (10) Mühlbauer, S.; Binz, B.; Jonietz, F.; Pfeleiderer, C.; Rosch, A.; Neubauer, A.; Georgii, R.; Böni, P. *Science* **2009**, *323*, 915.
- (11) Yu, X. Z.; Onose, Y.; Kanazawa, N.; Park, J. H.; Han, J. H.; Matsui, Y.; Nagaosa, N.; Tokura, Y. *Nature* **2010**, *465*, 901–904.
- (12) Duine, R. *Nat Nano* **2013**, *8*, 800–802.
- (13) Fert, A.; Cros, V.; Sampaio, J. *Nat Nano* **2013**, *8*, 152–156.
- (14) J., S.; V., C.; S., R.; A., T.; A., F. *Nat Nano* **2013**, *8*, 839–844.
- (15) Nagaosa, N.; Tokura, Y. *Nat Nano* **2013**, *8*, 899–911.
- (16) Rosch, A. *Nat Nano* **2017**, *12*, 103–104.
- (17) Jonietz, F.; Mühlbauer, S.; Pfeleiderer, C.; Neubauer, A.; Münzer, W.; Bauer, A.; Adams, T.; Georgii, R.; Böni, P.; Duine, R. A.; Everschor, K.; Garst, M.; Rosch, A. *Science* **2010**, *330*, 1648.

- (18) Parkin, S. S. P.; Hayashi, M.; Thomas, L. *Science* **2008**, *320*, 190.
- (19) Parkin, S.; Yang, S.-H. *Nat Nano* **2015**, *10*, 195–198.
- (20) Lin, Y. S.; Grundy, P. J.; Giess, E. A. *Applied Physics Letters* **1973**, *23*, 485–487.
- (21) Okubo, T.; Chung, S.; Kawamura, H. *Physical Review Letters* **2012**, *108*, 017206–.
- (22) Heinze, S.; von Bergmann, K.; Menzel, M.; Brede, J.; Kubetzka, A.; Wiesendanger, R.; Bihlmayer, G.; Blugel, S. *Nat Phys* **2011**, *7*, 713–718.
- (23) Dzyaloshinsky, I. *Journal of Physics and Chemistry of Solids* **1958**, *4*, 241–255.
- (24) Moriya, T. *Physical Review* **1960**, *120*, 91–98.
- (25) Fert, A.; Levy, P. M. *Physical Review Letters* **1980**, *44*, 1538–1541.
- (26) A.Fert, *Mater. Sci. Forum* **1980**, *59-60*, 439–480.
- (27) Ruderman, M. A.; Kittel, C. *Physical Review* **1954**, *96*, 99–102.
- (28) Kasuya, T. *Progress of Theoretical Physics* **1956**, *16*, 45–57.
- (29) Yosida, K. *Physical Review* **1957**, *106*, 893–898.
- (30) Imamura, H.; Bruno, P.; Utsumi, Y. *Physical Review B* **2004**, *69*, 121303–.
- (31) Kim, K.-W.; Lee, H.-W.; Lee, K.-J.; Stiles, M. D. *Physical Review Letters* **2013**, *111*, 216601–.
- (32) Banerjee, S.; Rowland, J.; Erten, O.; Randeria, M. *Physical Review X* **2014**, *4*, 031045–.
- (33) de Gennes, P. G. *Physical Review* **1960**, *118*, 141–154.
- (34) Calderón, M. J.; Brey, L. *Physical Review B* **2001**, *63*, 054421–.
- (35) Fernández-Rossier, J.; Brey, L. *Physical Review Letters* **2004**, *93*, 117201–.

- (36) Léger, Y.; Besombes, L.; Fernández-Rossier, J.; Maingault, L.; Mariette, H. *Physical Review Letters* **2006**, *97*, 107401–.
- (37) Subramanian, M. A.; Toby, B. H.; Ramirez, A. P.; Marshall, W. J.; Sleight, A. W.; Kwei, G. H. *Science* **1996**, *273*, 81.
- (38) Majumdar, P.; Littlewood, P. *Physical Review Letters* **1998**, *81*, 1314–1317.
- (39) Calderón, M. J.; Brey, L.; Littlewood, P. B. *Physical Review B* **2000**, *62*, 3368–3371.
- (40) Tatara, G.; Fukuyama, H. *Physical Review Letters* **1997**, *78*, 3773–3776.
- (41) Bruno, P.; Dugaev, V. K.; Taillefumier, M. *Physical Review Letters* **2004**, *93*, 096806–.
- (42) Finocchiaro, F.; Lado, J. L.; Fernandez-Rossier, J. *ArXiv e-prints* **2017**, 1702.06889.
- (43) Hamamoto, K.; Ezawa, M.; Nagaosa, N. *Physical Review B* **2015**, *92*, 115417–.
- (44) Hankiewicz, E. M.; Molenkamp, L. W.; Jungwirth, T.; Sinova, J. *Physical Review B* **2004**, *70*, 241301–.
- (45) Berg, B.; Lüscher, M. *Nuclear Physics B* **1981**, *190*, 412–424.
- (46) Slonczewski, J. C. *Journal of Magnetism and Magnetic Materials* **1996**, *159*, L1–L7.
- (47) Knoester, M. E.; Sinova, J.; Duine, R. A. *Physical Review B* **2014**, *89*, 064425–.
- (48) Hals, K. M. D.; Brataas, A. *Physical Review B* **2014**, *89*, 064426–.
- (49) Lin, S.-Z.; Reichhardt, C.; Batista, C. D.; Saxena, A. *Physical Review B* **2013**, *87*, 214419–.
- (50) Thiele, A. A. *Physical Review Letters* **1973**, *30*, 230–233.
- (51) Tretiakov, O. A.; Clarke, D.; Chern, G.-W.; Bazaliy, Y. B.; Tchernyshyov, O. *Physical Review Letters* **2008**, *100*, 127204–.

- (52) Díaz, S. A.; Troncoso, R. E. *Journal of Physics: Condensed Matter* **2016**, *28*, 426005.
- (53) Schulz, T.; Ritz, R.; Bauer, A.; Halder, M.; Wagner, M.; Franz, C.; Pfeleiderer, C.; Everschor, K.; Garst, M.; Rosch, A. *Nat Phys* **2012**, *8*, 301–304.
- (54) Jiang, W.; Zhang, X.; Yu, G.; Zhang, W.; Wang, X.; Benjamin Jungfleisch, M.; Pearson, J. E.; Cheng, X.; Heinonen, O.; Wang, K. L.; Zhou, Y.; Hoffmann, A.; te Velthuis, S. G. E. *Nat Phys* **2017**, *13*, 162–169.
- (55) Hurst, H. M.; Efimkin, D. K.; Zang, J.; Galitski, V. *Physical Review B* **2015**, *91*, 060401–.
- (56) Brey, L.; Calderón, M. J.; Das Sarma, S.; Guinea, F. *Physical Review B* **2006**, *74*, 094429–.
- (57) Freimuth, F.; Bamler, R.; Mokrousov, Y.; Rosch, A. *Physical Review B* **2013**, *88*, 214409–.
- (58) Krempaský, J. et al. **2016**, *7*, 13071 EP –.
- (59) Knoff, W.; Łusakowski, A.; Domagała, J. Z.; Minikayev, R.; Taliashvili, B.; Łusakowska, E.; Pieniążek, A.; Szczerbakow, A.; Story, T. *Journal of Applied Physics* **2015**, *118*, 113905.
- (60) Samarth, N. *Nature* **2017**, *546*, 216–218.
- (61) Gong, C.; Li, L.; Li, Z.; Ji, H.; Stern, A.; Xia, Y.; Cao, T.; Bao, W.; Wang, C.; Wang, Y.; Qiu, Z. Q.; Cava, R. J.; Louie, S. G.; Xia, J.; Zhang, X. *Nature* **2017**, *546*, 265–269.
- (62) Huang, B.; Clark, G.; Navarro-Moratalla, E.; Klein, D. R.; Cheng, R.; Seyler, K. L.; Zhong, D.; Schmidgall, E.; McGuire, M. A.; Cobden, D. H.; Yao, W.; Xiao, D.; Jarillo-Herrero, P.; Xu, X. *Nature* **2017**, *546*, 270–273.